Journal of Radiation Research and Applied Sciences 19 (2026) 102252

Contents lists available at ScienceDirect

Journal of Radiation Research and Applied Sciences

journal homepage: www.journals.elsevier.com/journal-of-radiation-research-and-applied-sciences

Modulated Arc Therapy (mARC) versus intensity-modulated radiation therapy in craniospinal irradiation: Evaluation of CT-slice-defined field junction thickness on dosimetric quality

E.A. Martín-Tovar *, A.H. Badillo-Alvarado, E.M. Hernández-Neri, L.E. Cocom-Poot

División de Oncología y Uronefrología, Departamento de Radioterapia, Unidad Médica de Alta Especialidad, Hospital de Especialidades del Centro Médico Nacional "Ignacio García Téllez", Instituto Mexicano del Seguro Social, CP 97150, Mérida, Yucatán, México

ARTICLE INFO

Keywords:
Modulated arc therapy (mARC)
Craniospinal irradiation
Intensity-Modulated Radiation Therapy (IMRT)
Field junction optimization
Dosimetric comparison

ABSTRACT

Background: One of the main technical challenges in craniospinal irradiation (CSI) is the risk of overdosing or underdosing in field overlap regions due to the need to match multiple treatment fields along the Planning Target Volume (PTV). To the authors' knowledge, the technical and dosimetric feasibility of modulated arc therapy (mARC) has not yet been evaluated for CSI. Unlike other arc techniques, mARC delivers dose in discrete arcs. This study compared mARC with intensity-modulated radiation therapy (IMRT) and analyzed the impact of overlap region thickness, defined by the number of computed tomography (CT) slices, on plan quality.

Methods: Treatment plans were generated for 10 patients using both mARC and IMRT on a Siemens Artiste linear accelerator. Optimization pseudo-structures were created with 4, 5, 6, and 7 tomographic slices at the craniothoracic and thoracolumbar junctions, resulting in eight plans per patient. The prescribed dose was 36 Gy in 20 fractions. Plans were evaluated by assessing PTV dosimetric parameters, doses to organs at risk (OARs), monitor units (MU), and treatment time. Statistical analysis employed two-way repeated-measures analysis of variance (ANOVA).

Results: The treatment technique was the main determinant of dosimetric outcomes. IMRT yielded lower mean dose values to certain OARs (kidneys, heart, lungs, and liver) and higher values for several PTV dose metrics. In contrast, mARC required fewer MUs and shorter treatment times and showed superior conformity and homogeneity indices. The number of CT slices did not produce statistically significant differences, and no significant technique–slice interactions were observed.

Conclusions: In CSI, the planning technique has a greater impact on dosimetric outcomes than the thickness of the overlapping field region. mARC improves efficiency in treatment time and MUs and provides improved conformity and homogeneity compared to IMRT. The number of tomographic slices has no impact on dosimetric quality.

1. Introduction

Craniospinal irradiation (CSI) is a radiotherapy technique in which the entire craniospinal axis is irradiated (Pollul et al., 2020). This is crucial for the treatment of certain central nervous system tumors such as medulloblastoma (Biltekin et al., 2021). The planning target volume (PTV) for this technique extends from the brain to the entire spinal length. This poses the main challenge in implementing CSI: the need to combine multiple treatment fields to homogeneously deliver the prescribed dose to the PTV. This commonly results under- or over-dosed regions in overlapping areas between fields, potentially compromising tumor control and the integrity of healthy tissues (Wang et al., 2018). There is a large number of publications where techniques for CSI are compared, such as volumetric modulated arc therapy (VMAT) (Tuong et al., 2025), intensity modulated radiation therapy (IMRT) (Özer et al., 2021), and 3D conformal radiation therapy (3D-CRT) (Studenski et al., 2013). These studies propose various solutions to optimize dosimetry in areas of field overlap. However, this problem persists due to its prevalence and clinical relevance.

Modulated arc therapy (mARC) is a hybrid intensity-modulated rotational irradiation technique, technically and functionally distinct from VMAT (V. Sarkar et al., 2015). Unlike VMAT, where radiation is

* Corresponding author.
E-mail address: enrique.martin.tovar@gmail.com (E.A. Martín-Tovar).

https://doi.org/10.1016/j.jrras.2026.102252
Received 16 December 2025; Received in revised form 18 February 2026; Accepted 22 February 2026

delivered continuously, mARC operates in a "burst" mode (Bell, Fleckenstein, et al., 2016; Dzierma, Bell, et al., 2014). In this mode, the dose is delivered in small arc segments called *"arclets,"* where the multi-leaf collimator (MLC) maintains a fixed configuration. These segments alternate with gaps in which no radiation is emitted, allowing the MLC leaves to reposition (Bell, Dzierma, et al., 2016; Luna & De Torres Olombrada, 2019). This feature gives mARC an advantage over VMAT, as irradiation in intermediate field configurations is not necessary, leading to better plan optimization (Choi et al., 2018). Another advantage of mARC is the ability to accurately determine the delivered dose at any given time, which is important in cases of treatment interruption (Dzierma, Nuesken, et al., 2014). The good dosimetric and technical performance of mARC treatments has been demonstrated for a wide variety of anatomical sites (Dzierma, Bell, et al., 2014; Dzierma et al., 2013; Dzierma, Nuesken, et al., 2014). However, to the best of the authors' knowledge, there are no previous studies that systematically evaluate the technical and dosimetric feasibility of mARC (which is technically distinct from VMAT) for craniospinal irradiation or compare it with other treatment techniques. This highlights the importance of this study as the first to explore the feasibility of mARC for CSI.

A particular problem in CSI planning is the field junction regions. Improper management of these regions can result in delivering an excessive or insufficient dose, which in turn could impact recurrence or late toxicity (Shafiq et al., 2009). An important variable to consider is the thickness of these junction regions, as it could affect the dosimetric quality of the plans. A novel way to control and evaluate this thickness is through pseudo-optimization structures, whose size can be defined by the number of tomographic slices used to construct them (e.g., 4, 5, 6, or 7 CT-slices). To the best of the authors' knowledge, there are no previous reports in the literature that systematically determine which junction region thickness (defined by the number of CT-slices) produces the best dosimetric results.

Therefore, this work has a twofold objective: First, to perform a dosimetric comparison between mARC and IMRT techniques in order to evaluate whether the former is technically feasible and capable of producing treatment plans with sufficient dosimetric quality to be clinically acceptable for CSI. And second, to analyze the influence of junction region thickness, defined by the number of tomographic slices, on the dosimetric quality of treatment plans, both for IMRT and mARC. The relevance of this work is twofold: on the one hand, it proposes a potentially superior technique available in treatment centers with limited resources in developing countries (such as Mexico), and on the other hand, it seeks to establish an optimization criterion for field junctions that can be reproducible and clinically beneficial.

2. Materials and methods

2.1. Delineation of target volumes and organs at risk

Ten patients with indication for CSI treated at the authors' practice were selected for retrospective evaluation. Patients ranged in age from 20 to 77 years, with a mean age of 32.9 years. Table 1 shows the patients' clinical and demographic characteristics. CT simulation was performed with head immobilization using a five-point thermoplastic mask, in the supine position with the arms positioned downward, parallel to the body. Images were acquired using a single-energy 64-slice Siemens SOMATOM Definition AS VA44A scanner (Siemens Healthineers, Germany). The axial slice thickness was 3 mm. All image data sets were then transferred to the Eclipse Treatment Planning System (TPS) (v. 16.1, Varian Medical Systems; Palo Alto, CA, USA). The entire brain, meninges, and spinal canal down to below the sacral vertebra S2, were contoured as a clinical target volume (CTV) (Ajithkumar et al., 2018). The PTV was generated by isotropically expanding the CTV by 5 mm. The heart, liver, esophagus, lungs, thyroid, kidneys, lens, and eyes were included as contoured organs at risk (OARs). A radiation oncologist delineated all the structures described above, and a second radiation oncologist reviewed and approved them. The prescribed dose was 36 Gy in 20 fractions (1.8 Gy per fraction). Dosimetric compliance criteria for PTV and OARs are shown in Table 2.

Table 1
Patient clinical and demographic characteristics for CSI treatment.

Patient	Gender	Age (years)	Diagnosis	PTV length (cm)
1	F	25	Acute Lymphoblastic Leukemia	65.27
2	F	41	Acute Lymphoblastic Leukemia	67.89
3	M	20	Medulloblastoma	67.43
4	M	77	Acute Lymphoblastic Leukemia	64.15
5	F	29	Acute Lymphoblastic Leukemia	67.98
6	M	25	Medulloblastoma	70.32
7	F	31	Acute Lymphoblastic Leukemia	66.92
8	M	28	Acute Lymphoblastic Leukemia	68.53
9	F	30	Acute Lymphoblastic Leukemia	65.19
10	M	23	Central nervous system extragonadal germ cell tumor	61.98

2.2. Planning techniques

The same medical physicist created eight treatment plans for all patients. These consisted of four IMRT plans and four mARC plans. For both techniques, each patient had a plan associated with optimization pseudo-structures with a different number of tomographic slices (4, 5, 6, and 7), resulting in eight plans in total. These pseudo-structures were used to control the dose distribution in the field junction regions by creating a controlled dose gradient. Three isocenters were placed along the craniospinal axis for each patient: one in the cranial region, one in the thoracic region, and the last in the lumbar region. All plans were normalized to ensure that 95% of the prescription dose covered 95% of the PTV. Treatment plans were calculated by the Eclipse TPS with the AAA (anisotropic analytical algorithm) on a Siemens Artiste linear accelerator with a 160 MLC (leaf width 5 mm at the isocenter), using 6 MV beams, and a dose grid size of 0.25 cm.

For mARC plans, four coplanar fields were used. The collimator angle was 0° for all fields. Each field had 180 control points (arclet length of 2°). The geometric configuration of the treatment fields used was adapted from a previous study (Prabhu et al., 2022). The cranial region of the PTV was covered with two arcs: one clockwise from 181° to 179° and another counterclockwise from 179° to 181°. The dorsal and lumbar regions of the PTV were treated with a single clockwise field each from 181° to 179°. To avoid irradiation of the patients' arms, two avoidance sectors were established in each of the fields corresponding to the dorsal and lumbar regions, using the same angular ranges in both cases (245°–270° and 90°–115°). Field sizes did not exceed the 15 cm recommended in the literature (Ugurlu & Temelli, 2020). The main priority of the optimization goals was adequate coverage of the PTV along with

Table 2
Dosimetric compliance criteria for PTV and OARs (Constine et al., 2024; Scoccianti et al., 2015; Vassantachart et al., 2023); $D_{1\%}$ - absorbed dose received by hottest 1% of planning target volume (PTV); $D_{95\%}$ - dose received by 95% of PTV; D_{mean} - mean dose; D_{max} - maximum dose.

PTV and OARs dosimetric compliance criteria	
PTV	$D_{1\%} < 38.52$ Gy
	$D_{95\%} > 34.20$ Gy
	35.28 Gy $< D_{mean} <$36.72 Gy
Heart	$D_{mean} < 15$ Gy
	$D_{max}<$30.60 Gy
Liver	$D_{mean} < 15$ Gy
Esophagus	$D_{mean} < 30$ Gy
Lung	$D_{mean} < 14$ Gy
Thyroid	$D_{mean} < 26$ Gy
Kidney	$D_{mean} < 15$ Gy
Lens	$D_{max}<$10 Gy
Eye	$D_{max}<$40 Gy

reducing the dose delivered to the OARs as much as possible. The field arrangement for the mARC plans can be seen in Fig. 1.

The IMRT plans utilized eleven coplanar fields. Their geometric distribution was adapted from a previous study (Hansen et al., 2015). The cranial PTV was covered by five fields with gantry angles of 60°, 100°, 0°, 300°, and 260°. The dorsal PTV was treated with three fields at 179°, 140°, and 220°, and the lumbar PTV with three identical fields. The collimator angle was 0° for all fields. The step-and-shoot technique was used with a maximum of 100 segments per field and a dose rate of 300 MU/minute (Andreas & Kundapur, 2015). To ensure a fair comparison, the same template and optimization goals were used as for the mARC plans. The field arrangement for the IMRT plans is shown in Fig. 2.

To minimize under- and overdosing in overlapping field regions, a dose gradient optimization technique based on a previous work was implemented (Myers et al., 2013). First, optimization pseudo-structures were generated in the craniothoracic and thoracolumbar junction regions. Each pseudo-structure was defined by the number of CT slices used for its creation (4, 5, 6, and 7 slices). Each treatment plan for both techniques used only structures with the same number of slices (same thickness), resulting in a gradual increase in the overlap area dimensions as thicker optimization structures were used. Subsequently, stepped dose targets were assigned to each pseudo-structure, such that they received 80%, 60%, 40%, and 20% of the prescribed dose, respectively. Fig. 3 shows the PTV regions (cranial, dorsal and lumbar) where the treatment fields overlap along with the optimization pseudo-structures marked with four different colors.

The optimization process was carried out sequentially, beginning with the fields corresponding to the cranial region of the PTV. The optimization objective was to deliver 100% of the prescribed dose to the PTV portion of that region, followed by a decreasing dose gradient in a caudal direction (80%, 60%, 40%, 20% to the cranial junction structures). Similarly, and independently, the fields corresponding to the lumbar region of the PTV were optimized to deliver 100% of the prescribed dose to the PTV of that region, along with a decreasing dose gradient in a cranial direction. This was done to create opposing and complementary dose profiles at each end of the dorsal region of the PTV.

Finally, the treatment fields corresponding to the dorsal region of the PTV were optimized using the sum of the previously calculated cranial and lumbar region plans as the base dose. In this final stage, the missing doses in each pseudo-structure are supplemented so that each one reaches 100% of the prescribed dose throughout the entire craniospinal volume. This process is illustrated in Fig. 3(b). The thickness of these gradient regions was systematically varied using different numbers of tomographic slices to evaluate their impact on the final dosimetric quality of the plan.

2.3. Dosimetric evaluation

A dose-volume histogram (DVH) was generated for the dosimetric analysis of PTVs and OARs. The homogeneity index (HI) was calculated with Eq. (1) (Wu et al., 2019):

$$HI = \frac{D_{2\%} - D_{98\%}}{D_{50\%}} \quad (1)$$

where $D_{2\%}$, $D_{98\%}$ and $D_{50\%}$ represent the absorbed doses received by 2% (near maximum dose), 98% (near minimum dose), and 50% of the volume of the PTV, respectively. A nearly homogeneous absorbed dose distribution will have a HI value close to 0.

The conformity index (CI) was also calculated (Eq. (2)) (Lin et al., 2015):

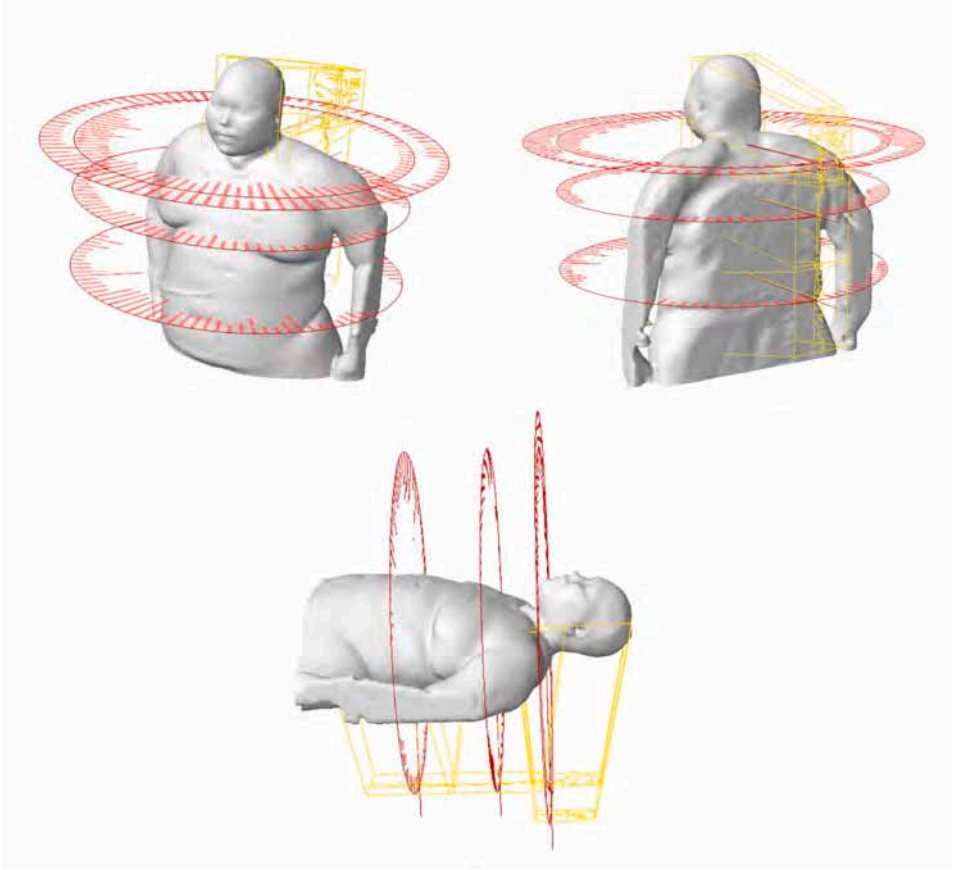

Fig. 1. Field arrangement for a single patient in modulated arc therapy (mARC) plans.

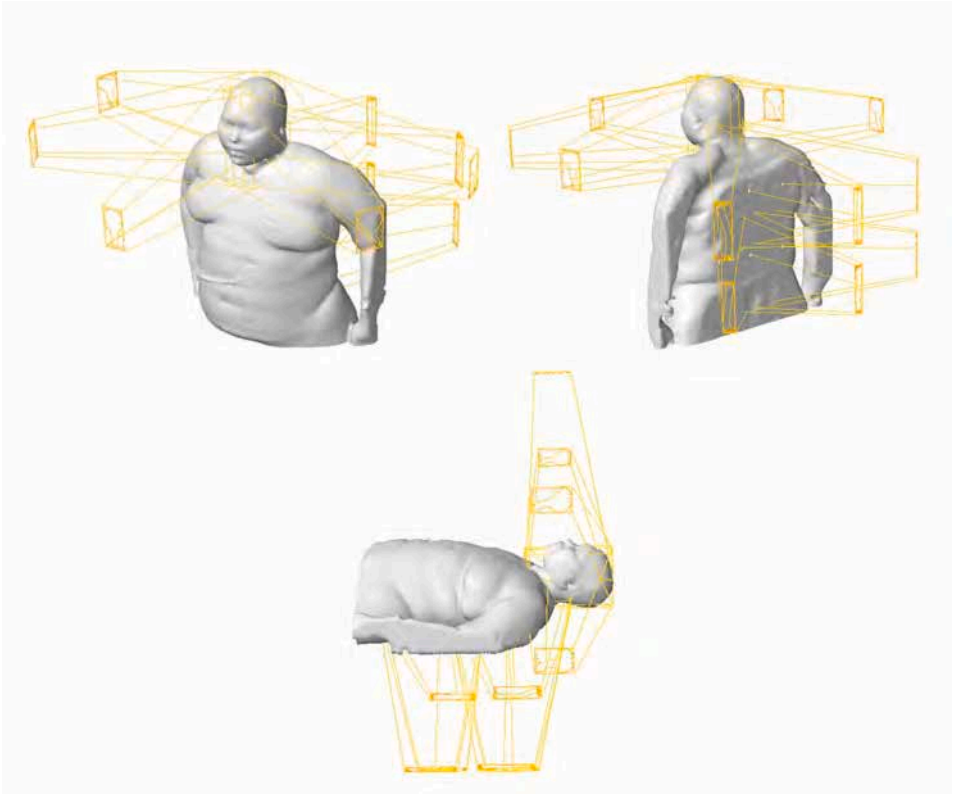

Fig. 2. Field arrangement for a single patient in intensity-modulated radiation therapy (IMRT) plans.

$$CI = \frac{V_{PTV,ref}}{V_{PTV}} \times \frac{V_{PTV,ref}}{V_{ref}} \quad (2)$$

where $V_{PTV,\ ref}$ refers to the volume of the 100% of the prescribed dose that covers the PTV, V_{PTV} refers to the volume of the PTV, and V_{ref} is the volume of the 100% prescribing dose curve. A CI value close to 1 indicates a dose distribution with almost ideal conformity. The treatment time in minutes was measured as the time interval in which the first to the last field was delivered including gantry rotation but excluding patient positioning. MUs were also recorded for the two types of treatment for comparison.

2.4. Statistical analysis

Statistical analysis was performed using a two-way repeated measures analysis of variance (ANOVA). The factors considered were the planning techniques (IMRT or mARC) and the number of tomographic slices used to construct the optimization pseudo-structures in the regions of field overlap (4, 5, 6, and 7). Normality was verified with Shapiro-Wilk tests, and the Mauchly test of sphericity was applied. When the sphericity criterion was not met, Greenhouse-Geisser corrections were applied. A statistical significance level of $p < 0.05$ was set. The statistical analyses were performed using OriginPro Software Version 2018 (OriginLab Corporation, Northampton, MA, USA).

3. Results

A senior radiation oncologist assessed the suitability of all treatment plans for the 10 patients. All plans were deemed clinically acceptable. The dose distribution for a single representative patient is shown in Fig. 4. Dose continuity in the overlap regions for both techniques is evident. An evaluation was performed by a senior radiation oncologist to determine if all the treatment plans for the 10 patients were adequate. All plans were deemed clinically acceptable. Visual inspection of the dose distribution for both techniques did not reveal a clear preference for either treatment technique. The mean PTV for the 10 patients was 2051.49 ± 401.53 cm^3 (range 1479.50–2877.20 cm^3). Table 3 shows measurements of plan quality (HI, CI, $D_{100\%}$, $D_{98\%}$, $D_{50\%}$, $D_{2\%}$, $D_{1\%}$, D_{mean}, and D_{max} for the PTV) and their standard deviations (SD). The *p*-values indicating statistical significance between the two planning techniques are in bold.

In general, the main factor affecting dosimetric results for the PTV was the planning technique. The thickness of the overlap regions (defined by the number of CT slices) did not show statistically significant effects. No significant interactions were observed between the two factors either. Both techniques presented dosimetric parameters within comparable ranges; however, mARC produced better conformity and homogeneity indices. Nevertheless, the absolute differences between all values are small and therefore lack clinical relevance.

The dosimetric parameters for the OARs are presented in Table 4. All plans for both techniques complied with the established dosimetric restrictions for the heart, lungs, liver, kidneys, esophagus, thyroid, lenses, and eyes. Consistent with the dosimetric parameters of the PTV, the planning technique had a significant impact on several OARs ($p < 0.05$), while neither the number of CT slices nor the technique × CT slices interaction showed statistically significant effects ($p > 0.05$). Compared with mARC, the IMRT technique tended to reduce the mean dose to several thoracic and abdominal organs, such as the lungs, liver, kidneys, and heart. Doses to ocular structures and other OARs were similar between both techniques and remained within clinically acceptable limits.

The MU values and treatment times are detailed in Table 5. Consistently, the results again show that it is the planning technique that has a significant impact on both parameters, since neither the number of CT-slices nor the interaction technique x CT-Slices showed statistical significance ($p > 0.05$). The total number of MU was consistently higher for IMRT (1208.02–1304.56 MU) than for mARC (951.88–994.92 MU), with an overall reduction of approximately 19–25% when using mARC ($p < 0.001$). Similarly, the treatment time was longer for IMRT

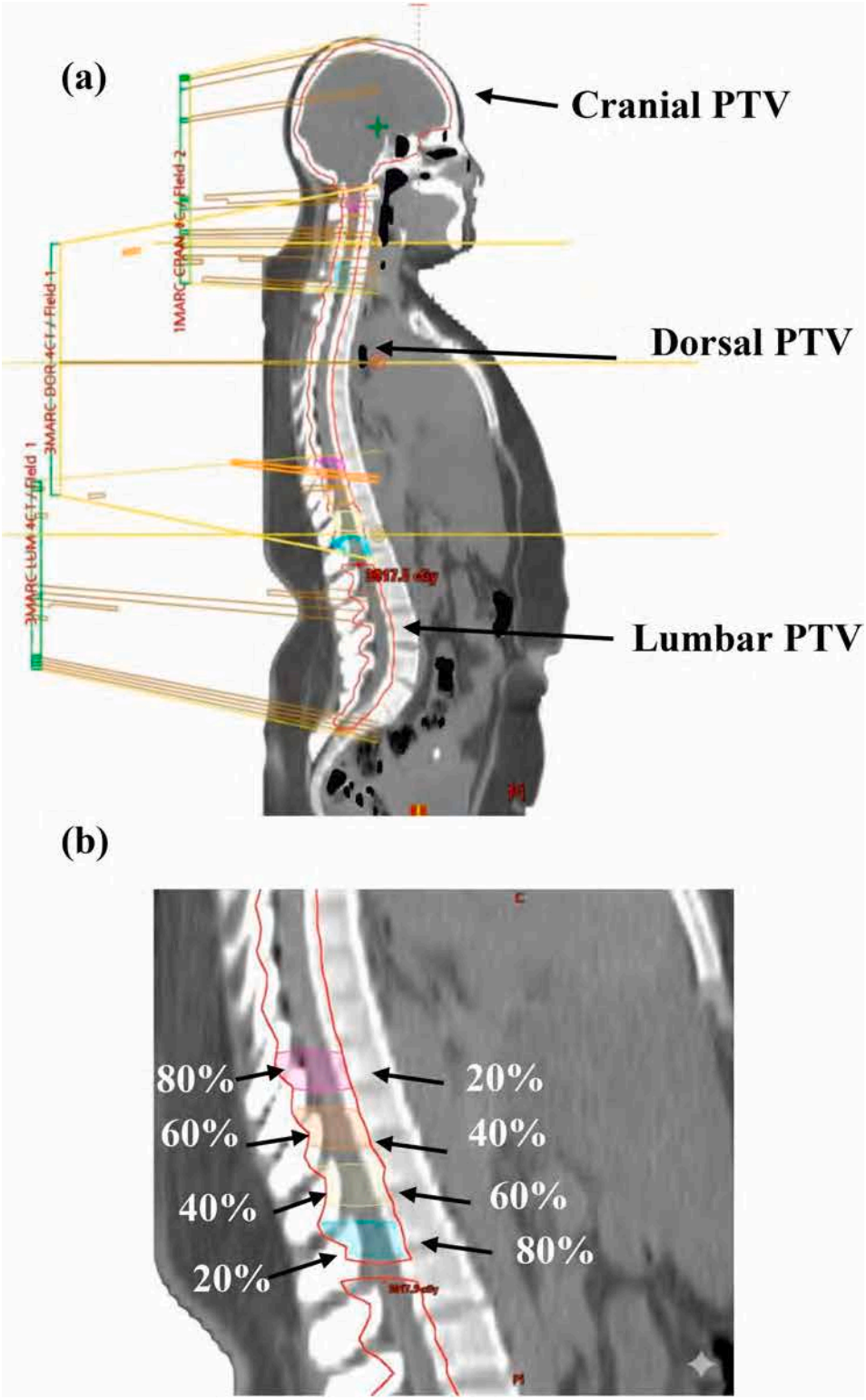

Fig. 3. (a) Patient used as an example showing the three distinct PTV regions (cranial, dorsal, and lumbar) along with the field overlap areas. (b) Zoom in of one the overlapping regions showing the optimization pseudo-structures and the percentage of prescription dose delivered to them for the entire craniospinal axis.

(241.62–260.91 s) than for mARC (190.38–198.98 s), with a reduction percentage ranging approximately from 19% to 25% ($p < 0.001$). Finally, representative DVHs for the PTV and selected OARs are shown in Fig. 5 for the 4C overlap configuration. This representative comparison was selected to improve visual clarity.

4. Discussion

This study demonstrates the feasibility of using mARC for CSI. Clinically acceptable results were obtained for both the PTV and OARs. Furthermore, the impact of the planning technique (mARC vs. IMRT) and of the CT slice-defined field junction on dosimetric outcomes was

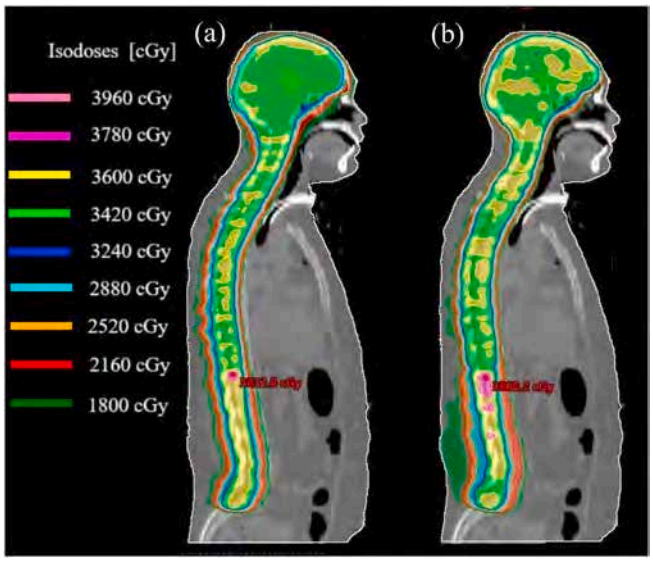

Fig. 4. Dose distribution for craniospinal irradiation in sagittal view for one patient: (a) modulated arc therapy (mARC) and (b) intensity-modulated radiation therapy (IMRT).

evaluated. To the best of the authors' knowledge, this is the first reported application of the mARC technique for CSI. The authors believe this could be a valuable contribution to the literature, as mARC is the least widely used arc therapy technique and could become a viable treatment alternative in radiotherapy departments equipped with a Siemens Artiste linear accelerator. Overall, mARC showed a slightly superior dosimetric performance compared to IMRT, with significant differences for several PTV and OAR parameters; however, the absolute values of these differences were minimal and likely lack significant clinical relevance. These results are consistent with previous studies comparing rotational planning techniques against IMRT (Hansen et al., 2015; Studenski et al., 2013; Özer et al., 2021). These studies state that continuous rotation techniques allow for finer angular modulation of extensive longitudinal structures such as in CSI. The mARC technique is mechanically distinct from VMAT, as the former uses discrete dose delivery sequences combined with simultaneous gantry movement. This delivery scheme may reduce unnecessary beam-on interruptions and promote smoother dose transitions along the neuraxis, depending on the specific system implementation. Although significant differences in absorbed doses were only observed for some OARs (heart, liver, lungs, thyroid, kidneys), the general trend was a reduction in doses to organs adjacent to highly modulated regions for IMRT plans. However, mARC kept the dose within clinically acceptable limits. This suggests that mARC does not compromise organ protection while exhibiting less dose dispersion, a behavior similar to previous studies comparing IMRT versus VMAT (Hansen et al., 2015; Studenski et al., 2013; Sun et al., 2019; Özer et al., 2021). One possible explanation for the observed dose differences to OARs is the use of oblique fields in IMRT plans (Biltekin et al., 2021). However, the technical characteristics of mARC could also have influenced both the dosimetric parameters of the PTV and the OARs, namely: minimization of abrupt repositionings due to its discrete dose delivery mode, which reduces field transitions and smooths axial gradients; native longitudinal segmentation, which reduces dosimetric variations between adjacent fields; lower dynamic aperture loading of the MLC, distributing modulation without requiring as many segments as IMRT; and more stable inverse optimization for elongated regions, which dilutes small target oscillations (Dzierma et al., 2016; Dzierma, Nuesken, et al., 2014; Luna & De Torres Olombrada, 2019; V. Sarkar et al., 2015). These properties would seem to explain the superiority of mARC over IMRT in terms of dose homogeneity and conformity, although the latter maintains advantages in specific localized regions. The efficiency of mARC derives more from its mechanical flow than from algorithmic complexity, unlike VMAT (Dzierma et al., 2015).

The main advantage of mARC over IMRT is a significant reduction in both treatment time and the number of MUs. In this study, an average reduction of approximately 22% (range: 19–25%) was observed in both MUs and treatment time for all evaluated cut configurations (4C to 7C). The greatest reduction was recorded at 5C (~25%) and the smallest at 4C (~19%). These results suggest that mARC is an effective option for delivering CSI treatment with clinically acceptable plans and a shorter treatment time. These findings are consistent with previous reports in the literature. Studies such as that by Dzierma et al. (Dzierma, Bell, et al., 2014; Dzierma et al., 2015, 2016; Dzierma, Nuesken, et al., 2014) reported a reduction in MUs of 22%, 20%, and 54% for patients with

Table 3
Dosimetric parameters of the planning target volume (PTV) for modulated arc therapy (mARC) and intensity-modulated radiation therapy (IMRT) across different numbers of CT slices (4C, 5C, 6C, 7C). Values are reported as mean ± standard deviation (SD). All plans were normalized such that 95% of the PTV received 3420 cGy. HI – homogeneity index (Eq. (1)); CI – conformity index (Eq. (2)). $D_{1\%}$ – dose received by the hottest 1% of the PTV; $D_{2\%}$ – dose received by the hottest 2%; $D_{50\%}$ – median dose; $D_{90\%}$ – dose covering 90% of the PTV; $D_{98\%}$ – dose received by 98% of the PTV; $D_{100\%}$ – minimum dose to the PTV; D_{max} – maximum dose; D_{mean} – mean dose.; *p*-values correspond to the main effects of technique, CT-slice number, and their interaction; bold *p*-values indicate statistical significance.

Item	Technique	4C (mean ± SD)	5C (mean ± SD)	6C (mean ± SD)	7C (mean ± SD)	*p*-value Technique	*p*-value CT-Slices	*p*-value Interaction
HI	mARC	0.0917 ± 0.0150	0.0912 ± 0.0099	0.0919 ± 0.0108	0.0971 ± 0.0112	**<0.001**	0.16	0.21
	IMRT	0.1116 ± 0.0143	0.1158 ± 0.0117	0.1180 ± 0.0173	0.1182 ± 0.0242			
CI	mARC	0.8995 ± 0.0112	0.9010 ± 0.0089	0.9022 ± 0.0103	0.8984 ± 0.0067	**<0.001**	0.33	0.30
	IMRT	0.8565 ± 0.0176	0.8543 ± 0.0150	0.8525 ± 0.0152	0.8494 ± 0.0255			
$D_{100\%}$ (cGy)	mARC	2643.96 ± 427.765	2584.81 ± 465.8541	2674.33 ± 419.4100	2629.66 ± 431.5673	**<0.001**	0.75	0.62
	IMRT	2145.31 ± 541.484	2182.04 ± 526.3442	2144.42 ± 537.8177	2141.61 ± 509.4232			
$D_{98\%}$ (cGy)	mARC	3367.65 ± 21.9816	3370.6 ± 15.0554	3376.59 ± 16.2894	3366.40 ± 21.4973	0.09	0.37	0.33
	IMRT	3388.95 ± 17.4246	3384.59 ± 21.0510	3380.16 ± 22.5660	3378.45 ± 30.5688			
$D_{90\%}$ (cGy)	mARC	3474.33 ± 6.4174	3471.87 ± 7.3725	3484.99 ± 30.5406	3472.79 ± 7.6426	0.28	0.27	0.51
	IMRT	3476.77 ± 12.3921	3480.66 ± 11.9365	3480.72 ± 13.4290	3479.70 ± 8.5570			
$D_{50\%}$ (cGy)	mARC	3557.51 ± 14.8654	3552.52 ± 14.9582	3562.02 ± 28.0901	3555.27 ± 17.0507	**0.002**	0.70	0.51
	IMRT	3581.88 ± 16.4055	3585.57 ± 15.8433	3584.91 ± 21.9865	3587.62 ± 22.2586			
$D_{2\%}$ (cGy)	mARC	3694.21 ± 41.722	3694.69 ± 30.8771	3704.20 ± 40.0945	3711.60 ± 38.4022	**0.006**	0.64	0.47
	IMRT	3788.72 ± 41.7423	3799.7 ± 32.3362	3803.20 ± 60.9220	3802.94 ± 61.0023			
$D_{1\%}$ (cGy)	mARC	3718.14 ± 43.0849	3719.1 ± 31.2925	3727.82 ± 39.3922	3736.90 ± 40.3545	**<0.001**	0.32	0.28
	IMRT	3825.22 ± 48.7141	3837.52 ± 40.9495	3827.43 ± 55.6121	3842.67 ± 65.0417			
D_{mean} (cGy)	mARC	3533.04 ± 64.2856	3548.98 ± 13.9940	3557.33 ± 26.0165	3551.91 ± 15.7116	**<0.001**	0.70	0.32
	IMRT	3582.6 ± 15.2996	3585.56 ± 15.6568	3584.32 ± 21.3970	3587.88 ± 22.5024			
D_{max} (cGy)	mARC	3849.59 ± 39.6747	3851.44 ± 38.2515	3858.38 ± 37.1652	3864.47 ± 62.6691	**<0.001**	0.69	0.55
	IMRT	4001.36 ± 74.7904	4008.08 ± 63.0238	4006.43 ± 69.9705	4029.77 ± 103.4334			

Table 4
Organs at risk (OARs) dosimetric parameters for modulated arc therapy (mARC) and intensity-modulated radiation therapy (IMRT) across different numbers of CT slices (4C, 5C, 6C, 7C). Values are reported as mean ± standard deviation (SD); D_{max} – maximum dose; D_{mean} – mean dose.; *p*-values correspond to the main effects of technique, CT-slice number, and their interaction; bold *p*-values indicate statistical significance.

Organ/ parameter	Technique	4C (mean ± SD)	5C (mean ± SD)	6C (mean ± SD)	7C (mean ± SD)	*p*-value Technique	*p*-value CT-Slices	*p*-value Interaction
Heart D_{max} (cGy)	mARC	1656.20 ± 612.486	1584.1 ± 613.496	1682.44 ± 611.809	1643.35 ± 568.573	**0.01**	0.64	0.75
	IMRT	1865.17 ± 711.060	1870.15 ± 683.845	1851.99 ± 683.489	1907.24 ± 790.580			
Heart D_{mean} (cGy)	mARC	729.124 ± 170.338	706.842 ± 174.810	747.488 ± 209.108	717.698 ± 218.690	**<0.001**	0.27	0.49
	IMRT	598.529 ± 203.832	618.509 ± 208.007	630.077 ± 204.412	608.075 ± 250.161			
Liver D_{mean} (cGy)	mARC	685.854 ± 144.095	714.349 ± 163.867	700.63 ± 157.722	689.481 ± 178.128	**<0.001**	0.07	0.18
	IMRT	424.026 ± 79.866	422.881 ± 80.126	423.807 ± 82.903	408.262 ± 98.528			
Esophagus D_{mean} (cGy)	mARC	1778.10 ± 478.050	1713.85 ± 487.620	1754.28 ± 488.318	1698.16 ± 536.691	0.10	0.15	0.30
	IMRT	1812.25 ± 373.231	1821.98 ± 537.788	1941.03 ± 606.796	1771.64 ± 686.154			
Left Lung D_{mean} (cGy)	mARC	644.736 ± 161.626	646.292 ± 171.459	650.379 ± 153.978	673.648 ± 150.992	**<0.001**	0.24	0.20
	IMRT	458.188 ± 118.158	476.228 ± 120.815	502.239 ± 123.713	491.812 ± 176.063			
Right Lung D_{mean} (cGy)	mARC	758.446 ± 163.662	776.062 ± 176.789	792.975 ± 169.522	791.73 ± 164.435	**<0.001**	0.13	0.12
	IMRT	549.356 ± 141.928	568.874 ± 149.691	595.76 ± 155.544	582.812 ± 217.098			
Thyroid D_{mean} (cGy)	mARC	1455.32 ± 309.277	1473.78 ± 312.391	1494.34 ± 336.287	1484.722 ± 355.620	**0.04**	0.35	0.55
	IMRT	1572.434 ± 373.231	1571.139 ± 344.485	1590.161 ± 343.441	1515.423 ± 452.081			
Left Kidney D_{mean} (cGy)	mARC	805.725 ± 214.659	804.529 ± 197.235	816.571 ± 266.957	776.905 ± 200.020	**0.001**	0.28	0.74
	IMRT	367.975 ± 129.124	368.052 ± 127.210	367.549 ± 123.376	359.77 ± 138.193			
Right Kidney D_{mean} (cGy)	mARC	920.604 ± 173.144	939.394 ± 219.895	895.316 ± 191.708	896.58 ± 243.920	**<0.001**	0.30	0.07
	IMRT	434.353 ± 140.924	432.311 ± 135.831	430.167 ± 130.576	422.383 ± 141.710			
Left Lens D_{max} (cGy)	mARC	708.11 ± 59.047	716.513 ± 69.355	688.521 ± 63.482	726.479 ± 120.354	0.64	0.97	0.95
	IMRT	725.974 ± 94.981	715.14 ± 93.452	753.018 ± 44.237	689.82 ± 136.615			
Right Lens D_{max} (cGy)	mARC	693.38 ± 40.785	680.84 ± 46.812	705.614 ± 72.022	704.111 ± 53.354	0.17	0.40	0.64
	IMRT	730.539 ± 96.279	733.556 ± 103.917	744.477 ± 46.323	708.129 ± 110.433			
Left eye D_{max} (cGy)	mARC	2746.232 ± 637.734	2767.771 ± 524.940	2715.506 ± 598.491	2767.403 ± 593.431	0.23	0.52	0.37
	IMRT	2609.581 ± 561.741	2710.27 ± 500.209	2677.867 ± 465.692	2620.01 ± 525.691			
Right eye D_{max} (cGy)	mARC	2782.942 ± 629.260	2817.658 ± 649.427	2860.756 ± 676.757	2885.069 ± 584.408	0.65	0.74	0.59
	IMRT	2852.574 ± 630.917	2854.228 ± 595.050	2853.625 ± 591.083	2856.605 ± 596.780			

Table 5
Monitor unit (MU) values and delivery time of treatment for IMRT and mARC; SD – standard deviation; *p*-values correspond to the main effects of technique, CT-slice number, and their interaction; bold *p*-values indicate statistical significance.

Item	Technique	4C (mean ± SD)	5C (mean ± SD)	6C (mean ± SD)	7C (mean ± SD)	p-value Technique	p-value CT-Slices	p-value Interaction
MUs	mARC	994.92 ± 128.712	979.99 ± 137.784	963.06 ± 149.231	951.88 ± 144.936	**<0.001**	0.25	0.6
	IMRT	1228.21 ± 121.672	1304.56 ± 62.670	1258.16 ± 120.967	1208.02 ± 82.098			
Time (s)	mARC	198.98 ± 25.743	196.15 ± 27.544	192.62 ± 29.86853	190.38 ± 28.976	**<0.001**	0.22	0.4
	IMRT	245.64 ± 24.334	260.91 ± 12.53284	251.63 ± 24.20124	241.62 ± 16.4225			

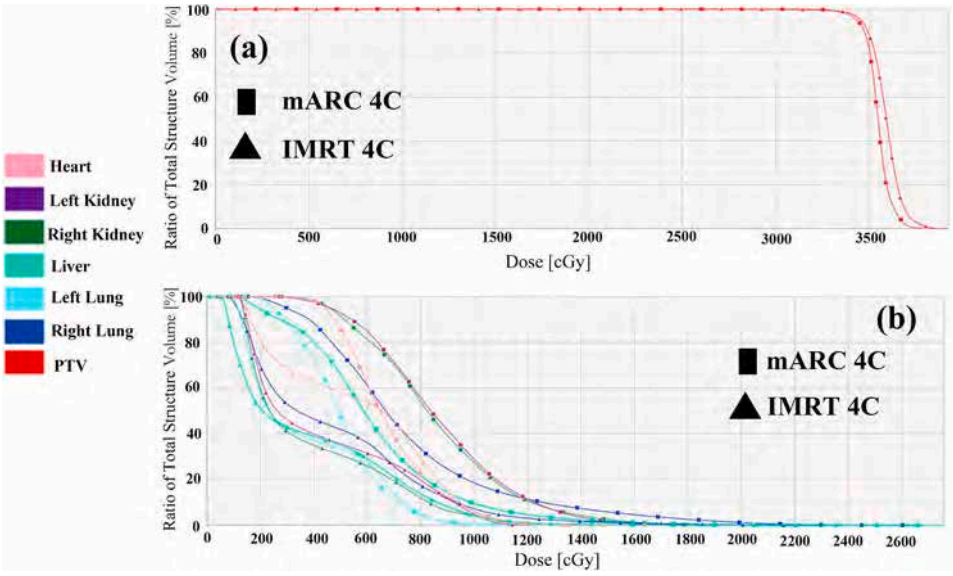

Fig. 5. DVHs grouped for visual clarity, showing a representative comparison between mARC and IMRT plans for the 4C overlap configuration: (a) PTV and (b) selected organs at risk. All plans were normalized such that 95% of the PTV received 3420 cGy. IMRT – intensity-modulated radiation therapy; mARC – modulated arc therapy.

prostate, head and neck, and hypopharyngeal cancer, respectively. These results also align with previous work by the authors evaluating mARC for a highly complex planning scenario such as hippocampal sparing whole brain radiotherapy (HS-WBRT) (Martín-Tovar et al., 2024). Bell et al. (Bell, Fleckenstein, et al., 2016) reported that treatment beams in mARC without a flattening filter (FFF) produce a reduction of 4 to 3 min in treatment times compared to IMRT. Such reductions in MUs and treatment duration have great clinical relevance, given that a higher number of MUs implies increases in scattered or filtered radiation outside the collimator (Hall & Wuu, 2003). Reducing the number of MUs lowers the risk of secondary cancers, which is particularly important in pediatric patients, who are more sensitive to the late effects of radiation (Hall, 2006; Seppala et al., 2009). Furthermore, a lower number of MUs results in shorter treatment times, which benefits both patients and the medical staff, reducing radiation exposure and optimizing resources (Petti et al., 2006). Finally, fewer MUs are generally associated with fewer adverse radiation effects, such as skin irritation, fatigue, better adherence to and tolerance of treatment, and an overall better quality of life (Barazzuol et al., 2020; Fowler et al., 2004; Pöll et al., 2008). The mARC technique limits radiation leakage due to its technical characteristics: continuous rotation fields, reduced collimator movement, and a smaller number of segments, which minimizes radiation leakage (Dzierma et al., 2013, 2016). In IMRT, the jaws in the treatment field are always fully open. In contrast, in mARC, the field aperture is dynamically adjusted, reducing beam scatter and leakage (Bell, Fleckenstein, et al., 2016). These technical differences could explain the differences in MUs and treatment times. IMRT generally requires a greater number of MUs, which is counterproductive, as it lengthens the time of each treatment session. This, in turn, can lead to patient discomfort, increase the risk of movement during irradiation, and compromise treatment accuracy (Lesnock et al., 2013). This work confirms what was reported in previous studies, that is, that the mARC technique produces shorter treatment times compared to IMRT.

To the best of the authors' knowledge, very few studies discuss the influence of overlap region thickness, defined by the number of CT slices, and its interaction with the treatment technique. In this study, no clinically significant dosimetric effects or technique × CT-slice interactions were identified. Although a slight tendency toward higher mean doses in some OARs was observed for larger overlap configurations, particularly for 6C, these differences were small, did not reach statistical significance, and are not considered clinically relevant within the evaluated range. Possible explanations include: longitudinal segmentation neutralizes volumetric interpolation variations; inverse optimization redistributes smoothed gradients between contiguous volumes; and in long regions such as the neuraxis, axial resolution effects are diluted by the dominant craniocaudal and sacral heterogeneity. These results appear to be consistent with previous literature indicating that only structures with abrupt dosimetric gradients show relevant sensitivity to resolution changes (Kry et al., 2013).

Numerous previous studies have evaluated the dosimetric performance of mARC in various anatomical regions (Salter et al., 2011; V. Sarkar et al., 2015). Kainz et al. (Kainz et al., 2011) compared mARC with tomotherapy and VMAT in patients with brain, head and neck, breast, and prostate tumors. Their study reported that mARC produces clinically acceptable treatment plans with dosimetric quality similar to the other two techniques mentioned. However, it has been established that, in general, both the number of monitor units (MUs) and treatment times are longer with mARC compared to VMAT. This has been attributed to the burst delivery mode, which interrupts beam delivery to allow movement of the MLC. Despite this, mARC offers greater flexibility in MLC configuration, as it allows for precise knowledge of the delivered dose at any time in the event of unforeseen interruptions (Dzierma, Nuesken, et al., 2014).

Table 6 compares the MUs obtained in this study with those reported in several other studies from the literature. In all subsequent studies, the dose prescription was identical to that of this work. It can be observed that, in general, the MU values are intermediate between those obtained for VMAT and IMRT, being higher than for VMAT but lower than for IMRT. Even in comparison with VMAT-based studies such as Sarkar et al. (B. Sarkar et al., 2020), slightly lower values were obtained in this work, further supporting the authors' interpretation. According to the authors' judgment, this establishes mARC as a valid treatment technique for implementation in CSI.

Table 6
Number of Monitor Units (MUs) of the present study and those reported in previously published studies for CSI; SD – standard deviation; IMRT – intensity-modulated radiation therapy; mARC – modulated arc therapy; VMAT – volumetric modulated arc therapy.

		mean ± SD		
	Number of patients	Technique	Number of beams	MU
Present study	10	mARC	4	Range: 951.88–994.92
(Özer et al., 2021)	11	VMAT	4	899.27 ± 120.178
(Özer et al., 2021)	11	IMRT	7	1264.82 ± 179.56
(Biltekin et al., 2021)	20	IMRT	11	1051.7 ± 377.0
(Hansen et al., 2015)	13	VMAT	2	916 ± 77
(Hansen et al., 2015)	13	IMRT	5	1617 ± 120
(Zhang et al., 2023)	12	VMAT	3	900.7 ± 156.5
(B. Sarkar et al., 2020)	10	VMAT	2	984 ± 123.4

There are many topics that could expand the knowledge contributed by this work on the application of mARC in CSI. There is still no consensus on which mARC technical parameters (length and number of arclets, angular separation, and MLC displacement) are optimal for achieving a better balance between dosimetric quality and treatment time efficiency. A systematic evaluation of these parameters in target volumes as extensive as those used in CSI could provide relevant information. Similarly, although this study did not find that the thickness of the overlap region, the number of tomographic slices, or the interaction between these slices and the treatment technique had any significant impact on dosimetric quality, it would be relevant to investigate other methods for smoothing and reinforcing the junction regions, especially in the face of possible positioning errors. This could answer whether the discrete firing mode of mARC is capable of producing more stable longitudinal dose gradients compared to techniques such as IMRT or VMAT.

Another interesting topic would be to study how different planning systems might modify the performance of mARC for CSI. Previous studies report that MUs and treatment times are influenced by the arclet generation algorithm (Dzierma et al., 2015). This would allow us to determine if the dosimetric advantages of mARC are dependent on the planning system used. Finally, it has been previously reported that the use of FFF beams in combination with the mARC technique can significantly reduce treatment times in other anatomical regions (Bell, Dzierma, et al., 2016). The PTV in CSI has a large volume; this option could provide additional clinical advantages.

5. Conclusions

This study evaluated the clinical feasibility of the mARC technique for craniospinal irradiation compared to IMRT, also considering the effect of overlap region thickness as defined by the number of CT slices. Both approaches yielded clinically acceptable treatment plans.

Compared to IMRT, mARC demonstrated equivalent dosimetry at the target volume level, with slight improvements in conformity and

homogeneity indices, and comparable doses to organs at risk. Furthermore, mARC allowed for a significant reduction in the number of monitor units and in treatment time.

No statistically significant differences were observed associated with the number of CT slices used in the overlap regions, nor were there any significant interactions between the planning technique and this parameter.

These results indicate that mARC is a viable and efficient alternative for planning craniospinal irradiation treatments.

CRediT authorship contribution statement

E.A. Martín-Tovar: Writing – review & editing, Writing – original draft, Supervision, Software, Project administration, Methodology, Investigation, Formal analysis, Data curation, Conceptualization. **A.H. Badillo-Alvarado:** Visualization, Validation, Supervision, Project administration, Methodology, Investigation, Formal analysis. **E.M. Hernández-Neri:** Visualization, Validation, Supervision, Methodology, Investigation, Formal analysis. **L.E. Cocom-Poot:** Software, Resources, Methodology, Investigation, Formal analysis, Data curation.

Consent for publication

All authors involved consent to publish work here within.

Ethical approval

This research work complies with the considerations issued in the Nuremberg Code, the Declaration of Helsinki promulgated in 1964 and its various modifications, including the update of Fortaleza, Brazil in 2013, as well as the international guidelines for medical research with human beings adopted by WHO and the Council for International Organizations for Research with Human Beings; In Mexico, it complies with the provisions of the General Health Law and the INAI (Instituto Nacional de Transparencia, Acceso a la Información y Protección de Datos Personales) on Research for Health and Protection of Personal Data, respectively.

Conflict of interest

The authors declare that they have no conflict of interest.

Acknowledgments

The authors thank the Radiotherapy Department (medical physicists, radiation oncologists, dosimetrists, radiation therapists, nurses and administrative personnel) of IMSS-UMAE Mérida for their work and invaluable collaboration.

References

Ajithkumar, T., Horan, G., Padovani, L., Thorp, N., Timmermann, B., Alapetite, C., Gandola, L., Ramos, M., Van Beek, K., Christiaens, M., Lassen-Ramshad, Y., Magelssen, H., Nilsson, K., Saran, F., Rombi, B., Kortmann, R., & Janssens, G. O. (2018). SIOPE – Brain tumor group consensus guideline on craniospinal target volume delineation for high-precision radiotherapy. *Radiotherapy & Oncology, 128*(2), 192–197. https://doi.org/10.1016/j.radonc.2018.04.016

Andreas, J. J. M., & Kundapur, V. (2015). Hippocampus avoidance whole-brain radiation therapy: A practical intensity-modulated radiation therapy planning and delivery approach to RTOG 0933. *Journal of Medical Imaging and Radiation Sciences, 46*(1), 78–84. https://doi.org/10.1016/j.jmir.2014.09.009

Barazzuol, L., Coppes, R. P., & van Luijk, P. (2020). Prevention and treatment of radiotherapy-induced side effects. *Molecular Oncology, 14*(7), 1538–1554. https://doi.org/10.1002/1878-0261.12750. John Wiley and Sons Ltd.

Bell, K., Dzierma, Y., Palm, J., Nuesken, F., Licht, N., & Rübe, C. (2016a). mARC prostate treatment planning with Varian Eclipse for flat vs. FFF beams. *Physica Medica, 32*(3), 474–478. https://doi.org/10.1016/j.ejmp.2016.02.011

Bell, K., Fleckenstein, J., Nuesken, F., Licht, N., Rube, C., & Dzierma, Y. (2016b). MARC treatment of hypopharynx carcinoma with flat and flattening-filter-free beam energies-a planning study. *PLoS One, 11*(10), 1–13. https://doi.org/10.1371/journal.pone.0164616

Biltekin, F., Yazici, G., & Ozyigit, G. (2021). A novel inverse optimization based three - dimensional conformal radiotherapy technique in craniospinal irradiation. *Physical and Engineering Sciences in Medicine, 44*(1), 265–275. https://doi.org/10.1007/s13246-021-00976-6

Choi, K. H., Kim, J., Lee, S. W., Kang, Y. N., & Jang, H. (2018). Dosimetric comparison between modulated arc therapy and static intensity modulated radiotherapy in thoracic esophageal cancer: A single institutional experience. *Radiation Oncology Journal, 36*(1), 63–70. https://doi.org/10.3857/roj.2017.00241

Constine, L. S., Marks, L. B., Milano, M. T., Ronckers, C. M., Jackson, A., Hudson, M. M., Marcus, K. J., Hodgson, D. C., Hua, C. H., Howell, R. M., Marples, B., Yorke, E., Olch, A., & Bentzen, S. M. (2024). A user's guide and summary of pediatric normal tissue effects in the clinic (PENTEC): Radiation dose-volume response for adverse effects after childhood cancer therapy and future directions. *International Journal of Radiation Oncology, Biology, Physics, 119*(2), 321–337. https://doi.org/10.1016/j.ijrobp.2023.09.005

Dzierma, Y., Bell, K., Palm, J., Nuesken, F., Licht, N., & Rübe, C. (2014a). *mARC vs . IMRT radiotherapy of the prostate with flat and flattening-filter-free beam energies* (Vols. 1–8).

Dzierma, Y., Licht, N., Norton, I., Nuesken, F., Rübe, C., & Fleckenstein, J. (2015). Konversion vom VMAT- zum Arclet-Plan im Bestrahlungsplanungssystem: Machbarkeit und dosimetrische Vergleiche zwischen VMAT, Arclets und Stehfeldbestrahlung. *Strahlentherapie und Onkologie, 191*(12), 961–969. https://doi.org/10.1007/s00066-015-0889-0

Dzierma, Y., Nuesken, F. G., Kremp, S., Palm, J., Licht, N. P., & Rübe, C. (2014b). Commissioning and first clinical application of mARC treatment. *Strahlentherapie und Onkologie, 190*(11), 1046–1052. https://doi.org/10.1007/s00066-014-0662-9

Dzierma, Y., Nuesken, F., Licht, N., & Rübe, C. (2016). Benchmarking the mARC performance – Treatment time and dosimetric linearity. *Zeitschrift Fβr Medizinische Physik, 26*(4), 339–348. https://doi.org/10.1016/j.zemedi.2016.02.001

Dzierma, Y., Nuesken, F., Licht, N., & Ruebe, C. (2013). A novel implementation of mARC treatment for non-dedicated planning systems using converted IMRT plans. *Radiation Oncology, 8*(1), 1–13. https://doi.org/10.1186/1748-717X-8-193

Fowler, J. F., Welsh, J. S., & Howard, S. P. (2004). Loss of biological effect in prolonged fraction delivery. *International Journal of Radiation Oncology, Biology, Physics, 59*(1), 242–249. https://doi.org/10.1016/j.ijrobp.2004.01.004

Hall, E. J. (2006). Intensity-modulated radiation therapy, protons, and the risk of second cancers. *International Journal of Radiation Oncology, Biology, Physics, 65*(1), 1–7. https://doi.org/10.1016/j.ijrobp.2006.01.027

Hall, E. J., & Wuu, C. S. (2003). Radiation-induced second cancers: The impact of 3D-CRT and IMRT. *International Journal of Radiation Oncology, Biology, Physics, 56*(1), 83–88. https://doi.org/10.1016/S0360-3016(03)00073-7

Hansen, A. T., Lukacova, S., Ph, D., Lassen-ramshad, Y., Ph, D., & Petersen, J. B. (2015). Comparison of a new noncoplanar intensity-modulated radiation therapy technique for craniospinal irradiation with 3 coplanar techniques. *Medical Dosimetry, 40*(4), 296–303. https://doi.org/10.1016/j.meddos.2015.03.007

Kainz, K., Chen, G. P., Chang, Y. W., Prah, D., Sharon Qi, X., Shukla, H. P., Stahl, J., & Allen Li, X. (2011). A planning and delivery study of a rotational IMRT technique with burst delivery. *Medical Physics, 38*(9), 5104–5118. https://doi.org/10.1118/1.3622612

Kry, S. F., Alvarez, P., Molineu, A., Amador, C., Galvin, J., & Followill, D. S. (2013). Algorithms used in heterogeneous dose calculations show systematic differences as measured with the radiological physics center's anthropomorphic thorax phantom used for RTOG credentialing. *International Journal of Radiation Oncology, Biology, Physics, 85*(1), e95–e100. https://doi.org/10.1016/j.ijrobp.2012.08.039

Lesnock, J. L., Farris, C., Beriwal, S., & Krivak, T. C. (2013). Upfront treatment of locally advanced cervical cancer with intensity modulated radiation therapy compared to four-field radiation therapy: A cost-effectiveness analysis. *Gynecologic Oncology, 129*(3), 574–579. https://doi.org/10.1016/j.ygyno.2013.02.012

Lin, J. F., Yeh, D. C., Yeh, H. L., Chang, C. F., & Lin, J. C. (2015). Dosimetric comparison of hybrid volumetric-modulated arc therapy, volumetric-modulated arc therapy, and intensity-modulated radiation therapy for left-sided early breast cancer. *Medical Dosimetry, 40*(3), 262–267. https://doi.org/10.1016/j.meddos.2015.05.003

Luna, R. B., & De Torres Olombrada, M. V. (2019). MARC preoperative rectal cancer treatments vs. 3D conformal radiotherapy. A dose distribution comparative study. *PLoS One, 14*(8), 1–16. https://doi.org/10.1371/journal.pone.0221262

Martín-Tovar, E. A., Badillo-Alvarado, A. H., Cocom-Poot, L. E., & Gaxiola-Sosa, J. L. (2024). Modulated Arc Therapy for hippocampal-avoidance whole brain radiation therapy: Planning comparison with intensity modulated Radiation Therapy. *Radiation and Environmental Biophysics*. https://doi.org/10.1007/s00411-024-01075-2

Myers, P., Stathakis, S., Mavroidis, P., Esquivel, C., & Papanikolaou, N. (2013). Evaluation of localization errors for craniospinal axis irradiation delivery using volume modulated arc therapy and proposal of a technique to minimize such errors. *Radiotherapy & Oncology, 108*(1), 107–113. https://doi.org/10.1016/j.radonc.2013.05.026

Özer, E. E., Çoban, Y., Turkan, T. S., Çifter, F., Karaçam, S., & Uzel, Ö. (2021). Dosimetric comparison of intensity-modulated radiation therapy and volumetric modulated arc therapy in craniospinal radiotherapy of. *Childhood, 36*(1), 96–103. https://doi.org/10.5505/tjo.2020.2381

Petti, P. L., Chuang, C. F., Smith, V., & Larson, D. A. (2006). Peripheral doses in CyberKnife radiosurgery. *Medical Physics, 33*(6), 1770–1779. https://doi.org/10.1118/1.2198173

Pöll, J. J., Hoogeman, M. S., Prévost, J. B., Nuyttens, J. J., Levendag, P. C., & Heijmen, B. J. (2008). Reducing monitor units for robotic radiosurgery by optimized

use of multiple collimators. *Medical Physics, 35*(6), 2294–2299. https://doi.org/10.1118/1.2919090

Pollul, G., Bostel, T., Grossmann, S., Akbaba, S., Karle, H., & Stockinger, M. (2020). Pediatric craniospinal irradiation with a short partial - Arc VMAT technique for medulloblastoma tumors in dosimetric comparison. *Radiation Oncology*, 1–10. https://doi.org/10.1186/s13014-020-01690-5

Prabhu, R. S., Dhakal, R., Piantino, M., Bahar, N., Meaders, K. S., Fasola, C. E., Ward, M. C., Heinzerling, J. H., Sumrall, A. L., & Burri, S. H. (2022). Volumetric Modulated Arc Therapy (VMAT) craniospinal irradiation (CSI) for children and adults: A practical guide for implementation. *Practical Radiation Oncology, 12*(2), e39–e47. https://doi.org/10.1016/j.prro.2021.11.005

Salter, B. J., Sarkar, V., Wang, B., Shukla, H., Szegedi, M., & Rassiah-szegedi, P. (2011). Rotational IMRT delivery using a digital linear accelerator in very high dose rate ' burst mode. *Physics in Medicine and Biology, 56*(7), 1931. https://doi.org/10.1088/0031-9155/56/7/002

Sarkar, V., Huang, L., Rassiah-Szegedi, P., Zhao, H., Huang, J., Szegedi, M., & Salter, B. J. (2015). Planning for mARC treatments with the Eclipse treatment planning system. *Journal of Applied Clinical Medical Physics, 16*(2), 458–464. https://doi.org/10.1120/jacmp.v16i2.5351

Sarkar, B., Munshi, A., Ganesh, T., Manikandan, A., & Mohanti, B. K. (2020). Dosimetric comparison of short and full arc in spinal PTV in volumetric-modulated arc therapy-based craniospinal irradiation. *Medical Dosimetry, 45*(1), 1–6. https://doi.org/10.1016/j.meddos.2019.03.003

Scoccianti, S., Detti, B., Gadda, D., Greto, D., Furfaro, I., Meacci, F., Simontacchi, G., Di Brina, L., Bonomo, P., Giacomelli, I., Meattini, I., Mangoni, M., Cappelli, S., Cassani, S., Talamonti, C., Bordi, L., & Livi, L. (2015). Organs at risk in the brain and their dose-constraints in adults and in children: A radiation oncologist's guide for delineation in everyday practice. *Radiotherapy & Oncology, 114*(2), 230–238. https://doi.org/10.1016/j.radonc.2015.01.016

Seppala, J., Lahtinen, T., & Kolmonen, P. (2009). Major reduction of monitor units with the avoidance of leaf-sequencing step by direct aperture based IMRT optimisation. *Acta Oncologica, 48*(3), 426–431. https://doi.org/10.1080/02841860802372264

Shafiq, J., Barton, M., Noble, D., Lemer, C., & Donaldson, L. J. (2009). An international review of patient safety measures in radiotherapy practice. *Radiotherapy & Oncology, 92*(1), 15–21. https://doi.org/10.1016/j.radonc.2009.03.007

Studenski, M. T., Shen, X., Yu, Y., Xiao, Y., Shi, W., Biswas, T., Werner-wasik, M., & Harrison, A. S. (2013). Intensity-modulated radiation therapy and volumetric-modulated arc therapy for adult craniospinal irradiation — A comparison with traditional techniques. *Medical Dosimetry, 38*, 48–54. https://doi.org/10.1016/j.meddos.2012.05.006

Sun, Y., Liu, G., Chen, W., Chen, T., Liu, P., Zeng, Q., Hong, J., & Wei, R. (2019). Dosimetric comparisons of craniospinal axis irradiation using helical tomotherapy, volume-modulated arc therapy and intensity-modulated radiotherapy for medulloblastoma. *Translational Cancer Research, 8*(1), 191–202. https://doi.org/10.21037/tcr.2019.01.30

Tuong, P. N., Duy, P. C., Van Thanh, N., Nguyen, L. T., Thao, M. T., Tai, D. T., Sandwall, P., Ashmeg, S., Sulieman, A., & Chow, J. C. L. (2025). Application of volumetric modulated arc therapy (VMAT) for craniospinal irradiation: Dosimetric analysis and clinical implementation. *Radiation Physics and Chemistry, 236*. https://doi.org/10.1016/j.radphyschem.2025.112965

Ugurlu, B. T., & Temelli, O. (2020). The impact of the field width on VMAT plan quality and the assessment of half field method. *Journal of Applied Clinical Medical Physics, 21*(3), 115–122. https://doi.org/10.1002/acm2.12834

Vassantachart, A., Olch, A. J., Jones, M., Marques, C., Ronckers, C., Constine, L. S., Maduro, J. H., de Boer, C., & Wong, K. (2023). A comprehensive review of 30 years of pediatric clinical trial radiotherapy dose constraints. *Pediatric Blood and Cancer, 70*(5), Article e30270. https://doi.org/10.1002/pbc.30270

Wang, K., Meng, H., Chen, J., Zhang, W., & Feng, Y. (2018). Plan quality and robustness in field junction region for craniospinal irradiation with VMAT. *Physica Medica, 48* (January), 21–26. https://doi.org/10.1016/j.ejmp.2018.03.007

Wu, Y., Zhu, B., Han, J., Xu, H., Gong, Z., Yang, Y., Huang, J., & Lu, E. (2019). A comparative dosimetric study of cervical cancer patients with para-aortic lymph node metastasis treated with volumetric modulated arc therapy vs. 9-field intensity-modulated radiation therapy. *Annals of Translational Medicine, 7*(22), 675. https://doi.org/10.21037/atm.2019.10.53, 675.

Zhang, Y., Huang, Y., Lin, J., Ding, S., Gong, X., Liu, Q., & Gong, C. (2023). Multi-isocenter VMAT craniospinal irradiation using feasibility dose-volume histogram-guided auto-planning technique. *Journal of Radiation Research, 64*(3), 612–621. https://doi.org/10.1093/jrr/rrad026